COMBINED SENSOR ASSEMBLY COMARS+ FOR EXOMARS EDM DEMONSTRATOR

A. Gülhan, T. Thiele, F. Siebe
Supersonic and Hypersonic Technology Department of the Institute of Aerodynamics and Flow Technology, German Aerospace Research Center (DLR), Linder Hoehe, D-51147 Cologne, Germany

ABSTRACT

Based on experience gained during the successful hypersonic flight experiments SHEFEX-I and SHEFEX-II using a combined aerothermal sensor package, the DLR Supersonic and Hypersonic Technology Department developed a new aerothermal sensor called COMARS. In addition to static pressure, surface temperature and total heat flux rate the COMARS sensor is also able to measure radiative heat fluxes using two fibre optic based gas radiation detectors of CNES (called ICOTOM). In addition to the COMARS sensors, the overall payload for the ExoMars EDM (Entry, Descent, Landing Demonstrator Module), called COMARS+, also contains a broad band radiometer of DLR. Furthermore a new electronic box containing multiplexer and power distribution units has been designed for the ExoMars mission.
The performed thermo-mechanical analysis shows that all necessary system requirements can be satisfied. The aerothermal tests performed in Martian atmosphere in the arc heated facility L2K demonstrated the ability of the COMARS+ payload to collect data even at low aerothermal loads which are present during Mars entry.

1. INTRODUCTION

For the design margin of spacecraft structures the reliability of the aerothermal predictions and qualification tools is essential. Ground testing facilities are not capable to reproduce the exact flight environment of the ExoMars EDM capsule, which will enter the Martian atmosphere in 2016. The CFD codes have shortcomings in terms of correct physical modeling of some critical aspects like back cover heating. In the back cover region of the vehicle the Reynolds number of the flow is low and the flow itself has a highly transient character. This results in low convective heat fluxes on the back cover heat shield. Another very important parameter is the high radiative heating resulting from excitation of carbon dioxide molecules behind the strong bow shock. In the base region the radiative heat flux is even higher than the convective one. But neither ground test facilities nor numerical tools can simulate the radiation environment completely. Therefore the European Space Agency (ESA) decided to instrument the back cover of the ExoMars EDM to measure total and radiative heat flux.
Based on the flight instrumentation experience of the flight experiments SHEFEX-I and SHEFEX-II the Supersonic and Hypersonic Technology Department of the German Aerospace Center (DLR) in Cologne has developed the combined aerothermal sensor COMARS. A sensor similar in composition provided excellent data during the SHEFEX-II flight in 2012 [1], [2]. The COMARS sensor unit allows measuring the total heat flux rate, surface temperature and pressure in one plug. Furthermore, for the ExoMars EDM the COMARS sensor also contains two spectral radiometers to measure the gas radiation. These spectral radiometers based on fibre optics were developed by CNES (called ICOTOM). In addition to the spectral radiometers integrated in the COMARS sensor, a separate broad band radiometer of DLR measures the total radiative heat flux. The complete DLR payload including COMARS and radiometer sensors and the corresponding analogue data processing unit is called COMARS+.
This paper describes the main properties of the COMARS+ payload, mechanical and thermal design details and finally the results of aerothermal tests performed at DLR Cologne.

2. PAYLOAD LAYOUT

The following table presents an overview of the different parts of the DLR ExoMars EDM back cover instrumentation (COMARS+ payload). The payload consists of overall three COMARS sensors, one broad band radiometer, an electronic box and the corresponding harness between sensors and electronic box. The electronic box (multiplexing signal conditioner) is thereby used for sensor signal conditioning and multiplexing for acquisition by the EDM Remote Terminal Power Unit (RTPU). For the pressure measurement a Pirani-type pressure sensor is used. The total heat flux is measured by a heat flux microsensor from the VATELL company which also incorporates a temperature sensor. The radiative heat flux at two different spectral bands is measured by the ICOTOM sensors developed by CNES.

Unit name	Description
Multiplexing Signal Conditioner (MSC)	Electronic box
COMARS1 (COM 1)	Combined static pressure, total heat-flux, temperature and two CNES spectral radiometer sensors (ICOTOM)
COMARS2 (COM 2)	
COMARS3 (COM 3)	
Radiometer (RAD 1)	Broad band radiometer
Payload harness	Harness connecting the sensors to the electronic box

Table 1: COMARS+ payload instrumentation overview

The COMARS sensor is fixed to the ExoMars back cover (BCV) structure using a honeycomb insert to which the COMARS sensor is screwed with four M4 screws. Figure 1 and Figure 2 show exterior and interior views of the COMARS sensor with denomination of the different parts.

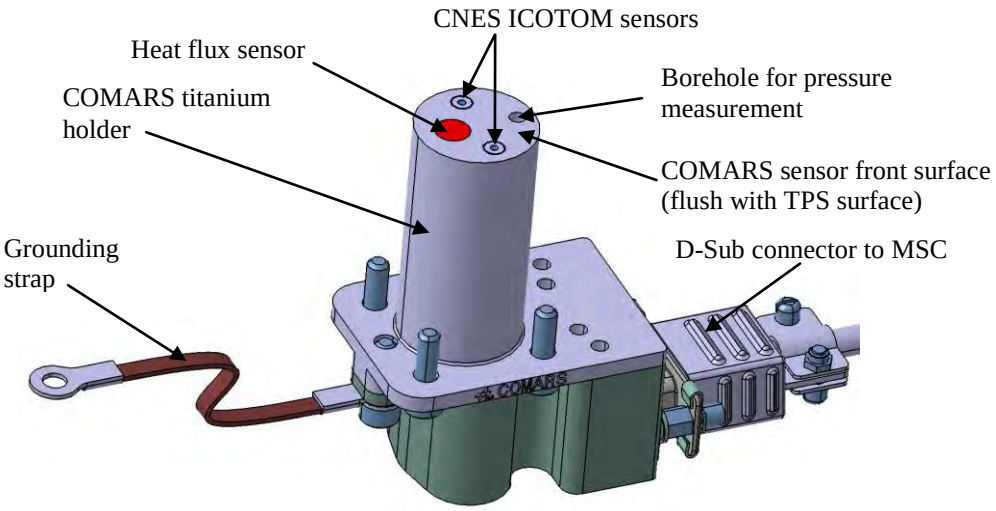

Figure 1: COMARS sensor assembly (top view)

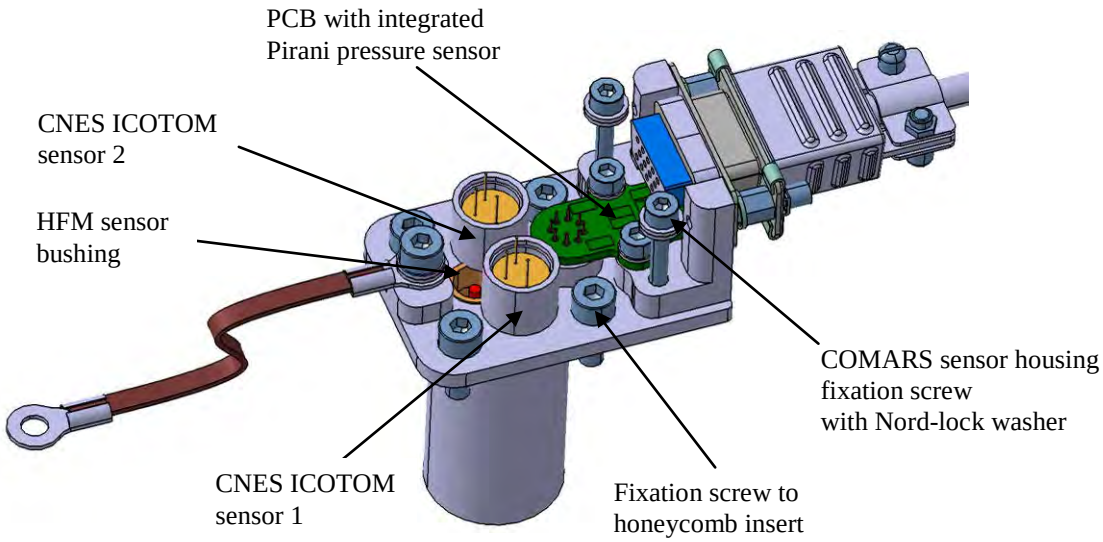

Figure 2: COMARS sensor assembly (bottom view with removed housing)

The multiplexing signal conditioner (COMARS+ electronic box) is used to amplify the signals of the sensors and to multiplex these signals on three analogue output lines for acquisition by the RTPU. It consists of one multiplexing board and one power board which generates the necessary voltage levels from the unregulated bus of the EDM using a DC/DC converter. The sensor signal multiplexing is controlled via clock and synchronisation signals coming from the EDM RTPU. Figure 3 shows an exterior and interior view (with removed cover plate) of the MSC box.

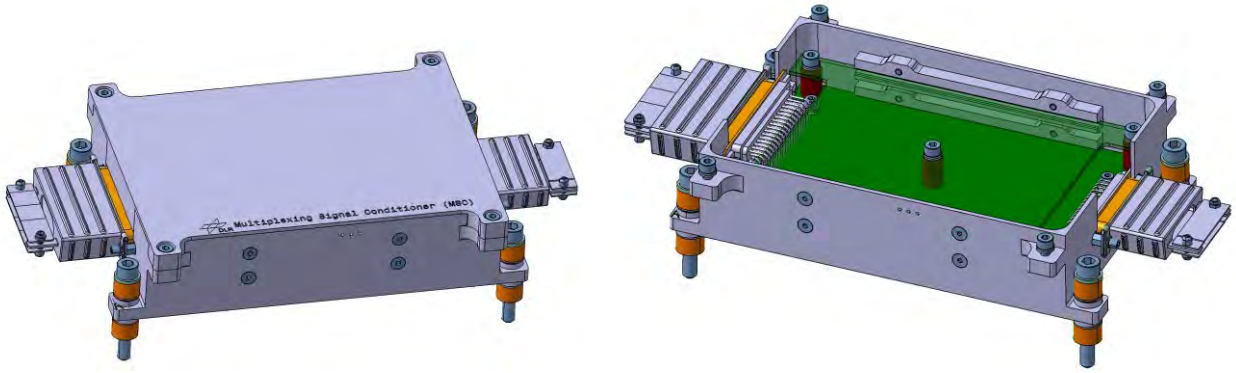

Figure 3: Electronic box of the COMARS+ payload

In Figure 4 the multiplexing layout for the COMARS+ payload is shown. The multiplexing board has three multiplexing units, one for each analogue channel (ChA-ChC). Each multiplexer handles the data of one sensor unit and one housekeeping signal (HK1-HK3).

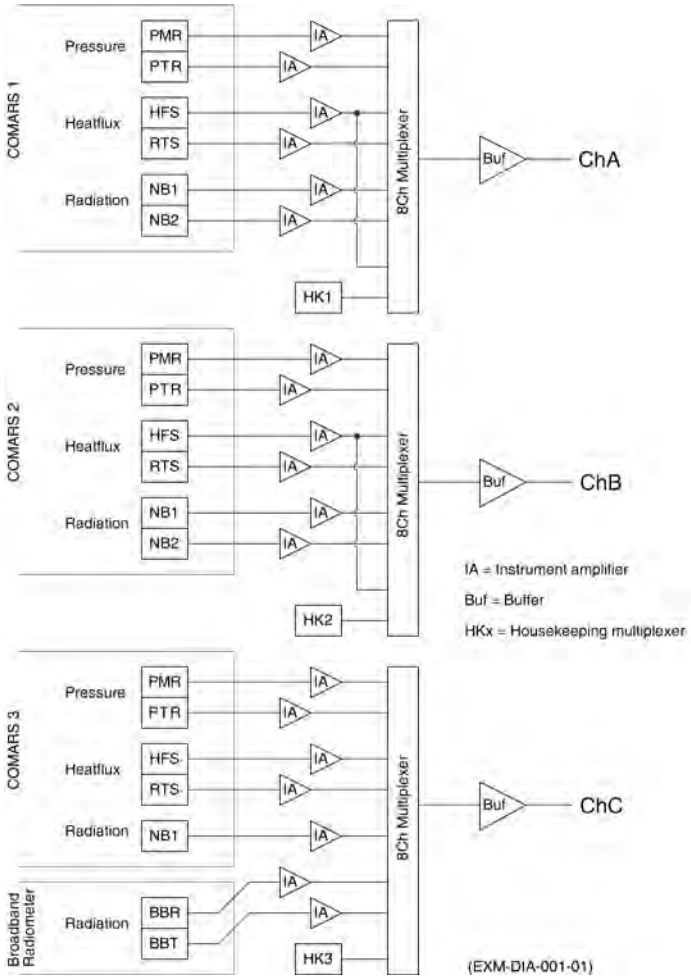

Figure 4: Data handling layout of COMARS+

The amplification of the sensor signals is thereby done before the multiplexing process (Instrument Amplifiers shown in Figure 4). The Pirani-pressure sensors provides two signals, the actual pressure signal (PMR) and the pressure sensor temperature (PTR) which is also used as temperature reference for the ICOTOM sensors. The Vatell heat flux sensors measure the heat flux rate (HFS) and surface temperature (RTS) of the sensor front surface. The ICOTOM sensors of CNES generate two signals corresponding to the radiative heat fluxes at the two wavelengths bands (NB1 and NB2). Since the third multiplexer has to process the radiation (BBR) and temperature signals (BBT) of the DLR broad band radiometer, only one ICOTOM signal (NB1) of COMARS sensor 3 is multiplexed.
In the following figure the location of the COMARS+ components on the inner side of the ExoMars EDM back cover structure is shown.

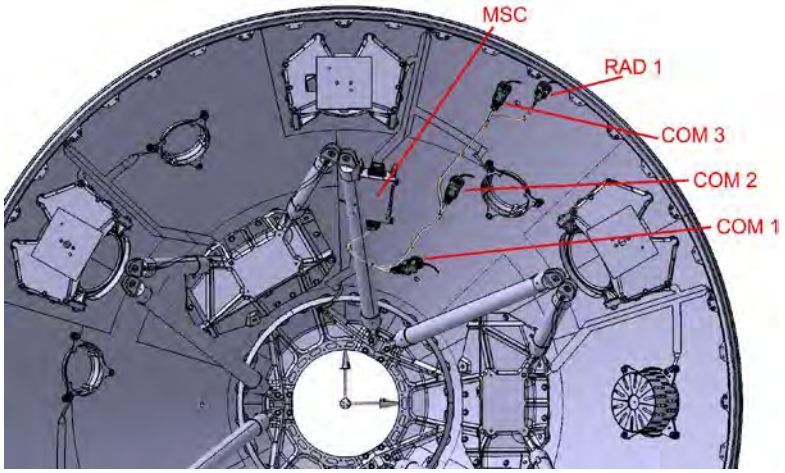

Figure 5: COMARS+ sensors and electronic box location on ExoMars back cover

3. STRUCTURAL ANALYSIS

To verify the structural integrity of the COMARS+ components during the launch phase several structural analysis were performed. In the following some results of the numerical analysis for the COMARS+ electronic box are shown. The electronic box is the heaviest part of the payload (about 800 grams) and is therefore exposed to the highest mechanical stresses acting on box structure and fixation devices (screws).
To evaluate the worst case vibration loads during launch and ascent, the random vibration spectra for the COMARS+ MSC is used (Figure 6). These random loads are converted into static loads using the Miles-equation. Using this equation a static load curve can be derived for the MSC which is also shown in Figure 6 with a maximum g-load of 182 g in out-of-plane (OOP) and 33 g in in-plane (IP) direction.

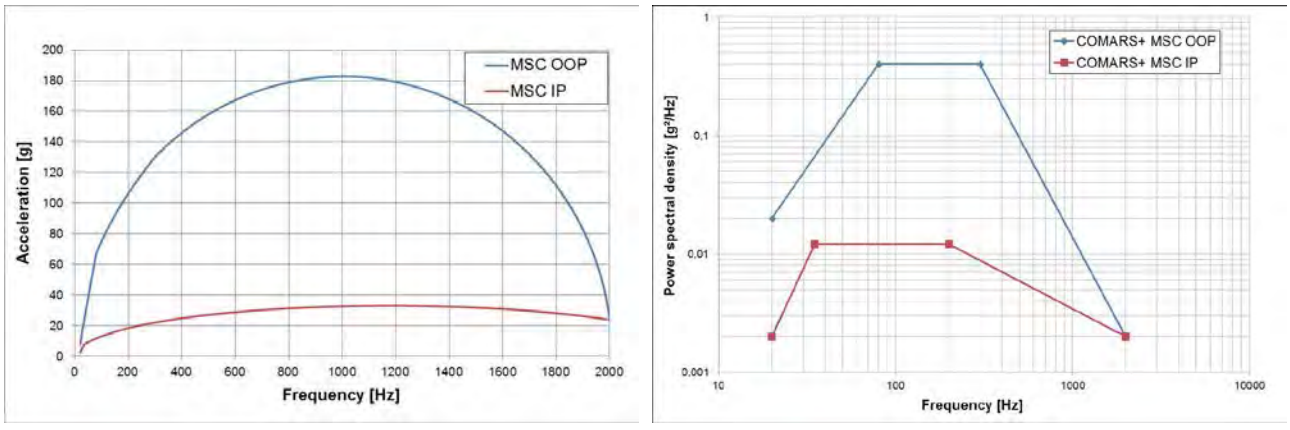

Figure 6: COMARS+ MSC static load curve (left) derived from random vibration loads (right)
(taken from ExoMars EDM mechanical environment specification)

The FEM-model of the MSC is shown in Figure 7. For the FEM-model some simplifications were made but the overall mass of the box was kept constant:

- The geometry of the D-Sub connectors attached to the box was simplified but their mass was kept constant.
- Due to their small mass impact the harness cables attached to the connectors and the grounding strap of the box were neglected.
- All internal fixation screws (PCBs, connectors…) were removed to decrease the overall number of necessary mesh points. Although the overall mass of the internal fixation screws is small, the mass of the box structure was slightly increased to compensate for the missing weight.
- All contacts between different box parts are set to be bonded contacts.
- The multiplexing board and the power board are modelled as solid parts made of FR4 material (glass-reinforced epoxy laminate). The material density was increased to get the correct mass values for the boards. Therefore a uniform mass distribution is assumed on the PCBs.

A screw preload force of 6500 N (according to the used mounting torque, screw strength and thread friction coefficient) was applied to all four MSC fixation screws. To evaluate the static loads used for the simulation with a sufficient safety margin, a box mass of 1 kg and the maximum accelerations of 182 g and 33 g were used. This lead to an acceleration of 1820 m/s^2 in OOP direction and an acceleration of 330 m/s^2 in IP direction. The used FEM-mesh shown in Figure 7 consisted of 3506942 nodes and 1987165 elements.

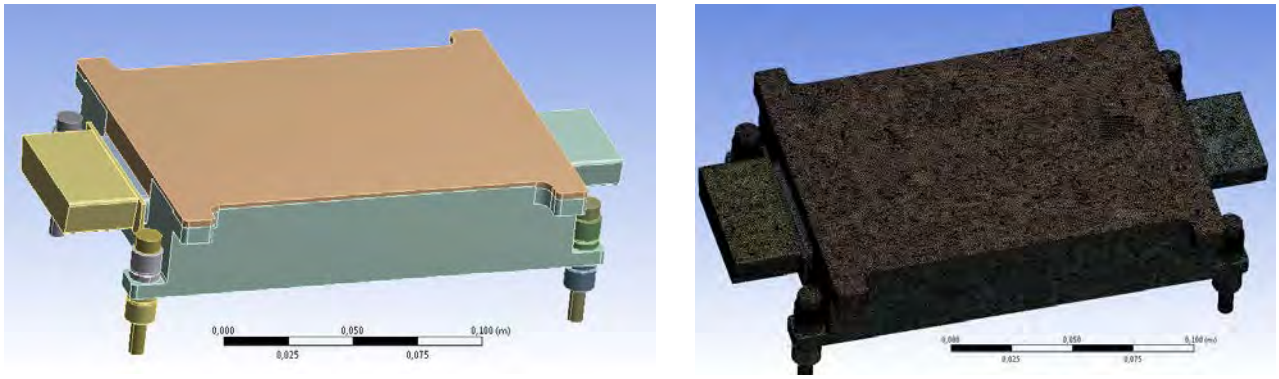

Figure 7: FEM-model and mesh

Figure *8* shows the von Mises equivalent stress for the MSC bottom part. The maximum stress of about 95 MPa occurs at the mounting feet. The MSC bottom part is manufactured from Aluminium material (7075 T7351) with yield strength ($R_{p0.2}$) of 380 MPa which ensures enough margin to prevent breaking or plastic deformation of the material. The maximum calculated stress inside the fixation screw shafts was calculated to 340 MPa. The yield strength for the used stainless steel screws (strength class 80) is 600 MPa which indicates sufficient margin to prevent plastic deformation of the MSC fixation screws.

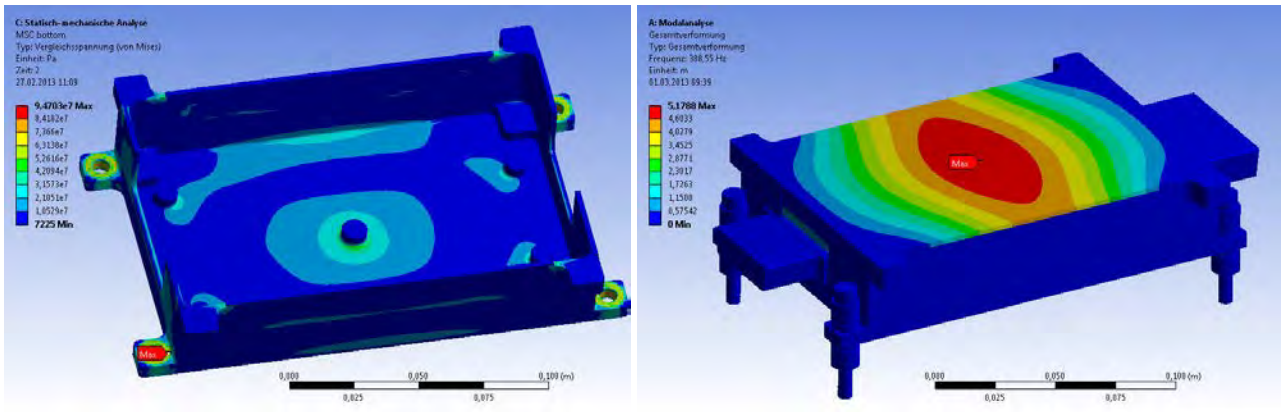

Figure 8: Von Mises equivalent stress at MSC bottom part (left) and modal analysis of MSC box (right)

The calculated stresses for the other fixation components (e.g. thermal washers) are also well inside the corresponding material stress limits. In addition to the structural analysis a modal analysis was also performed for the MSC to determine the first fundamental frequency. The result is also shown in Figure 8 with the first fundamental frequency at 388 Hz, which corresponds with the vibration of the MSC cover plate.
To determine the maximum deflection of the PCBs inside the MSC box a Power Spectral Density (PSD) analysis was performed using the random vibration loads shown in Figure 6. The result of the MSC modal-analysis was used as input for the PSD analysis. Figure 9 shows the deflection of the multiplexing and power board perpendicular to the board plane. A scaling factor of 3σ was used for the analysis leading to a result probability of 99.7%.
The maximum deflection of the multiplexing board occurs around the center of the board. As a fixation screw is placed in the center of the PCB, the deflection is very small with a maximum deflection of 0.11 mm. This is well inside the tolerable range to prevent damage or detachment of electronic components.
The maximum deflection of the power board is larger with a maximum of 0.36 mm at the short sides. This is because the power board is not fixed to the MSC structure by D-Sub connectors at these sides (like the multiplexing board). But this deflection is still inside the tolerable deflection range. In addition to the soldering, the components on the power board (DC/DC converter, voltage filter) are fixed to the PCB with epoxy adhesive. This is mainly done because of the quite severe shock loads that occur at the stage separations during ascent. Furthermore, these components are placed near the center of the board where the deflections are lower due to the fixation point (screw) in the center of the PCB.

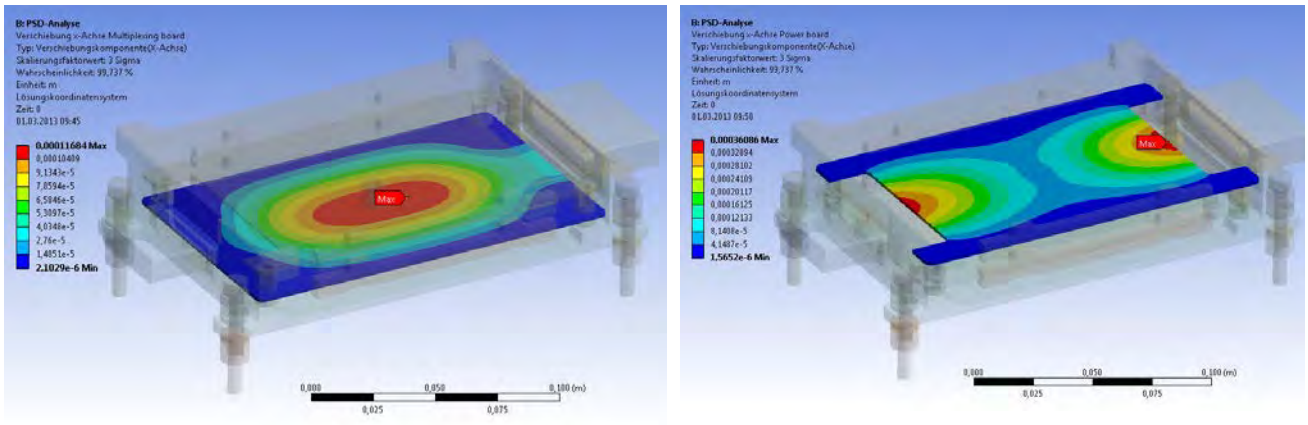

Figure 9: MSC PSD analysis, deflection of the multiplexing board (left) and power board (right)

4. THERMAL ANALYSIS

To verify the temperature resistance of the COMARS sensor assembly during Mars entry transient thermal analysis have been performed. The used thermal model is shown in Figure 10 and consists of a cut-out of the TPS with an area of 90x90 mm with integrated COMARS sensor. The components of the thermal model are (see Figure 1 and Figure 2)

- TPS with nominal thickness of 7.6 mm.
- Honeycomb structure with a thickness of 25 mm. The honeycomb structure was modelled as a solid structure with adjusted material properties (density, thermal conductivity, specific heat capacity).
- Honeycomb insert (to which the COMARS sensor is fixed) made of Aluminium material.
- Epoxy glue between honeycomb insert and honeycomb structure.
- COMARS titanium holder.
- Heat flux sensor (HFM).
- ICOTOM sensor without detector.

The glue between the TPS, carbon skins and honeycomb as well as the carbon skins themselves (at the upper and lower side of the honeycomb) were not included. These parts would normally increase the thermal resistance between TPS and sensor. Therefore the thermal environment for the COMARS sensor is even more severe if these parts are omitted. Furthermore, all other COMARS sensor parts were neglected because they are located at the back end of the sensor and do not influence the heat conduction from the TPS to the lower parts of the sensor along the sensor axis. All contacts between the different parts were assumed to be bonded contacts. The most susceptible parts of the COMARS sensor concerning temperature are the Pirani pressure sensor, the ICOTOM detectors and the heat flux sensor. To evaluate the

temperature of the Pirani pressure sensor and ICOTOM detectors, the temperature of the corresponding sensor contact surface to the titanium holder is calculated (see also Figure 10). The heat flux sensor consists of several parts. At the sensor front end the sensor substrate, on which the thermopile for the heat flux measurement is deposited, may be exposed to a maximum temperature of 200°C. Epoxy glue directly behind the substrate is used for the electric cable fixation, at which substrate and epoxy glue are encapsulated by a nickel housing.

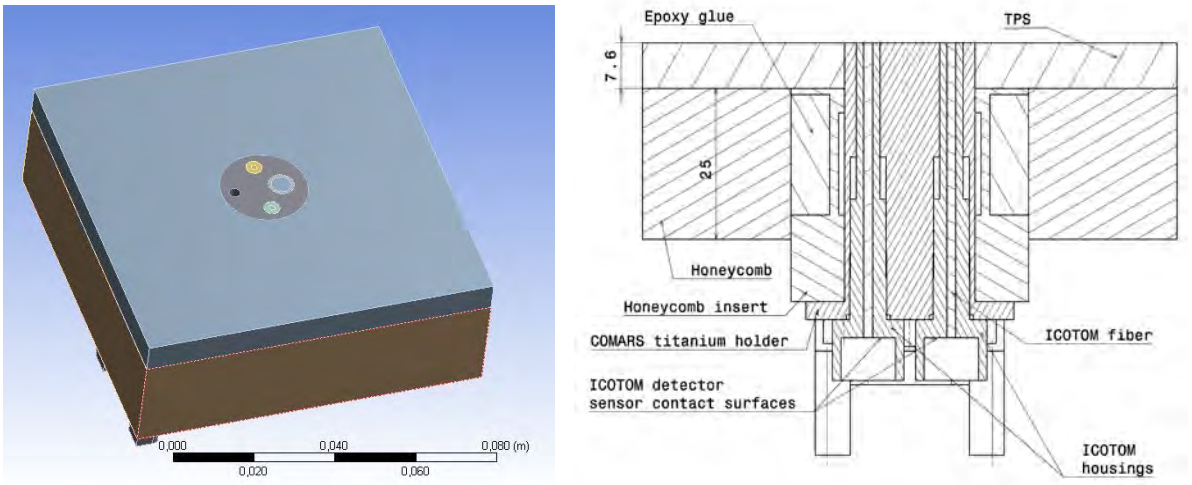

Figure 10: Simplified thermal model for COMARS sensor thermal analysis

The heat flux used for the thermal analysis can be seen in Figure 11 and was taken from the ExoMars EDM aerothermodynamic database. The COMARS and DLR radiometer sensors are thereby located in zones V and VI according to Figure 11. The shown heat flux profiles were computed with a wall temperature of 300 K and represent the worst-case heat fluxes to the TPS (sizing case). As the heat flux in zone VI is slightly higher than in zone V, the heat flux of zone VI was used for the thermal simulations.

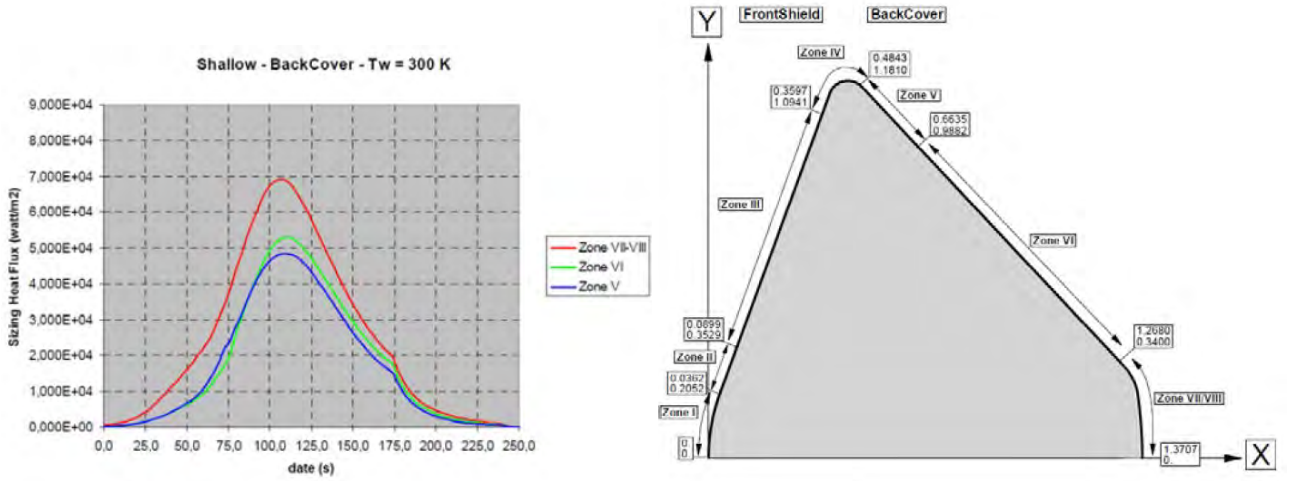

Figure 11: Sizing heat flux profile for EDM back cover TPS and EDM zone definition
(taken from ExoMars EDM aerothermodynamic database)

The heat flux was applied to the upper TPS surface including the COMARS sensor surface. To simulate further heat conduction into the material after the heat flux becomes zero, the simulation time of the thermal analysis was extended to 450 seconds. A radiation to ambient space (temperature -120°C) with an emissivity of 0.9 was assumed for the TPS surface. Radiation of the COMARS sensor to ambient space was neglected. All other outer surfaces were set to be adiabatic. A uniform starting temperature of 300 K was used for the simulation to be compliant with the wall temperature assumption used for the heat flux calculation. In Figure 12 the used FEM mesh is shown in a sectional view

with overall 626065 knots and 281982 elements. The temperature distribution inside the sensor at the end of the simulation is also shown in Figure 12. As can be seen in the figure, the distribution inside the sensor is nearly homogeneous with a temperature of about 75°C.

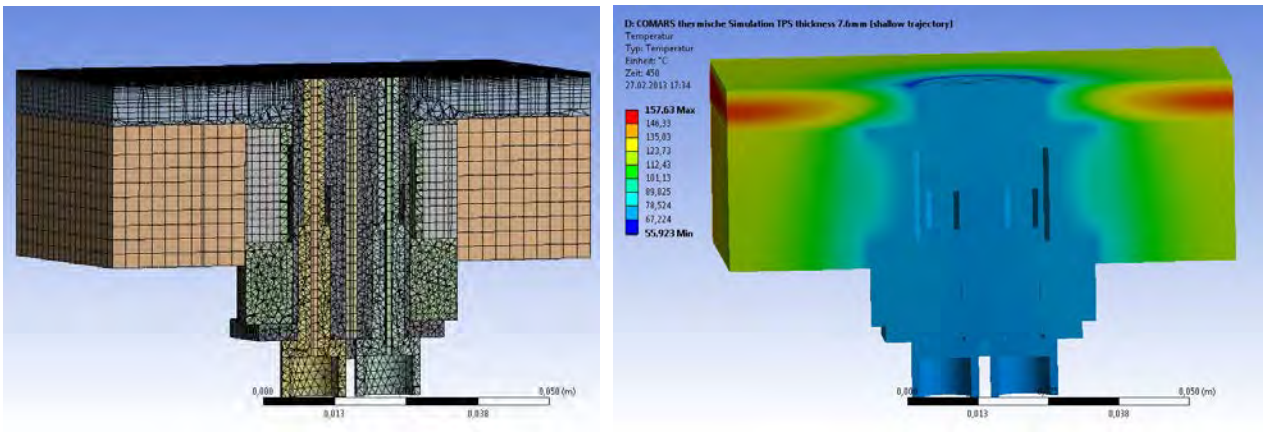

Figure 12: FEM mesh for COMARS simulation and computed temperature distribution at simulation end (t=450s)

The resulting maximum temperatures of the different parts are presented in Figure 13. The outer surface of the TPS reaches a maximum temperature of nearly 650°C, whereas the titanium holder of the COMARS sensor only heats up to a maximum of 126°C due to the heat sink effect of the metallic sensor components. As already shown in Figure 12, all sensor parts are at a nearly homogeneous temperature level at the end of the simulation time.

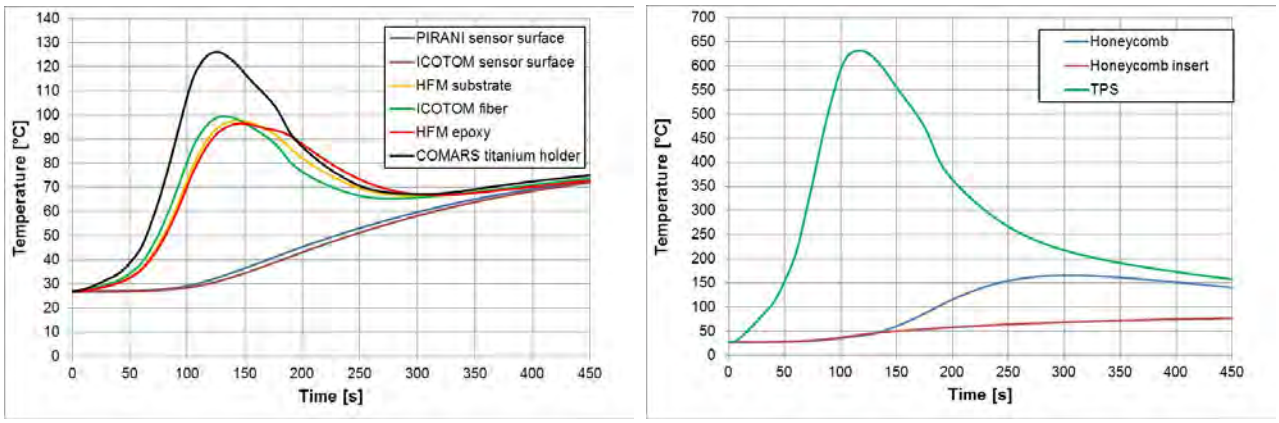

Figure 13: COMARS thermal simulation maximum temperatures

In the following table the important temperatures of the COMARS parts are summarized and compared with the maximum operative range. All calculated values are below the maximum operative temperatures which ensures, that the COMARS sensor is capable to withstand the thermal environment during Mars entry.

Part / surface	Maximum calculated temperature [°C]	Maximum operative temperature [°C]
Pirani sensor	72	90
ICOTOM detector	72	75
HFM substrate	98	200
HFM epoxy	96	200
ICOTOM fiber at TPS	99	> 120
COMARS titanium holder	126	400

Table 2: Calculation results compared with maximum operative temperatures of the different COMARS parts

As some of the calculated temperatures are very close to the corresponding maximum operative range, the following remarks should be considered:

- The used simulation time is longer than the measurement time of the sensor and therefore the temperatures at the actual end of the measurement will be lower.
- The starting temperatures of the different parts will be much lower than 300 K at the beginning of Mars entry leading to lower temperatures at the end of the measurement time.
- Some simplifications were made to the thermal model that would, in reality, decrease the calculated temperatures (e.g. omission of glue between TPS and honeycomb and assumption of overall bonded contacts between the different parts with perfect heat conduction).
- The used heat flux profile taken from the ExoMars EDM aerothermodynamic database represents the back cover TPS sizing case and therefore already includes a safety margin.

Considering all these points, the actual temperatures during Mars entry will definitely be lower than the calculated ones shown in Table 2 and therefore enough safety margin for the COMARS sensor is provided.

To verify that the implementation of the COMARS sensor into the TPS will not lead to local overheating of the TPS or honeycomb structure, a further simulation was performed only for the TPS structure using the same heat flux levels presented in Figure 11. A comparison of the TPS and honeycomb temperatures with and without COMARS sensor is shown in Figure 14. The curves show the maximum temperatures of the lower surface of the TPS (intersection to the honeycomb) and of the lower surface of the honeycomb structure (inner side of back cover). As can be seen in the figure, the maximum temperature of the lower TPS surface is higher without a COMARS sensor. The same is true for the lower surface of the honeycomb structure. Therefore the integration of the COMARS sensor into the TPS does not cause local overheating of the TPS or honeycomb structure. In fact, the temperatures are even lower with a COMARS sensor due to a local heat sink effect.

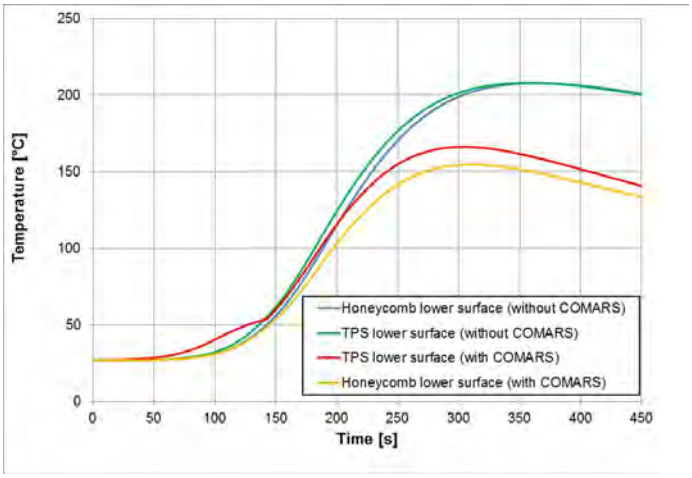

Figure 14: TPS temperatures with and without COMARS sensor

A thermal simulation was also performed for the DLR broad band radiometer. The thermal model consists of a cut-out of the TPS with an area of 90x90 mm with integrated radiometer sensor. For TPS and honeycomb structure the same simplifications were made as for the COMARS sensor. The only parts of the radiometer which were incorporated in the thermal model are the titanium holder and the thermopile sensor which is located at the lower end of the conical borehole, see Figure 15. The thermopile sensor was thereby replaced by a circular sensor dummy at the contact surface between titanium holder and thermopile. The temperature of the upper surface of this sensor dummy represents the temperature to which the thermopile sensor is exposed during Mars entry. All other parts (fixation screws, housing) were removed because they do not influence the heat conduction from the TPS to the lower parts of the sensor along the sensor axis and therefore have a negligible effect on the thermopile temperature calculation.
The temperature distribution inside the radiometer sensor at the end of the simulation is shown in Figure 15. As can be seen in the figure, the complete radiometer sensor has a nearly uniform temperature distribution of about 93°C.

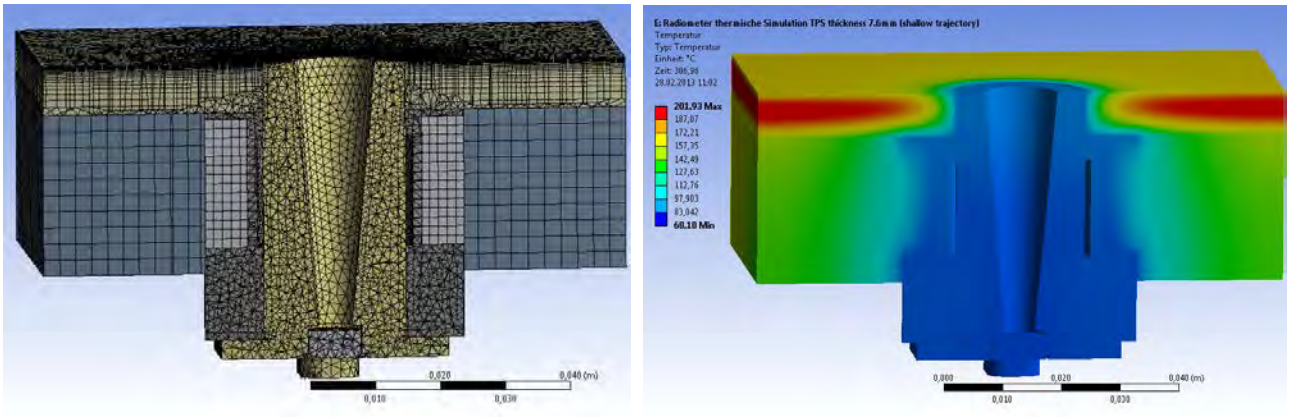

Figure 15: FEM mesh for radiometer simulation and computed temperature distribution at simulation end (t=450s)

Figure 16 shows the results for the radiometer computation. The diagrams show the maximum temperatures for the radiometer parts (thermopile sensor, radiometer titanium holder) and for the TPS parts (TPS, honeycomb, honeycomb insert). A maximum temperature of 93°C is reached for the thermopile sensor at the end of the simulation. With a maximum working temperature of 180°C, the calculated temperature is thereby well inside the operative temperature range of the sensor.

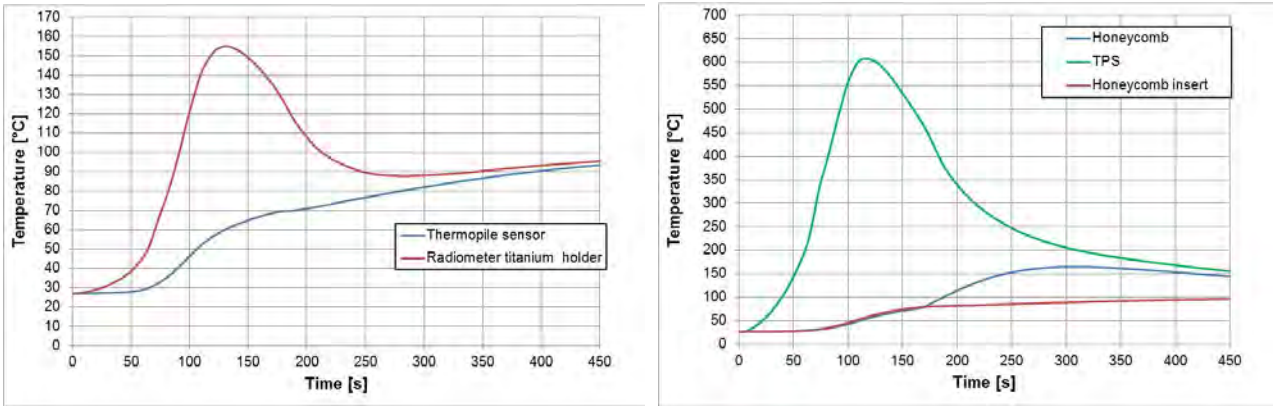

Figure 16: Calculated maximum temperatures for radiometer thermal simulation

5. AEROTHERMAL TESTS

All tests have been performed in the L2K facility of the Supersonic and Hypersonic Technology Department of DLR Cologne [3,4] . In contrast to preliminary stagnation point tests, these aerothermal tests were carried out in a flat plat configuration (Figure 17). The COMARS sensor and the broad band radiometer were integrated into the holder at the same distance from the model holder nose tip. This guarantees the same flow conditions on both sensors.

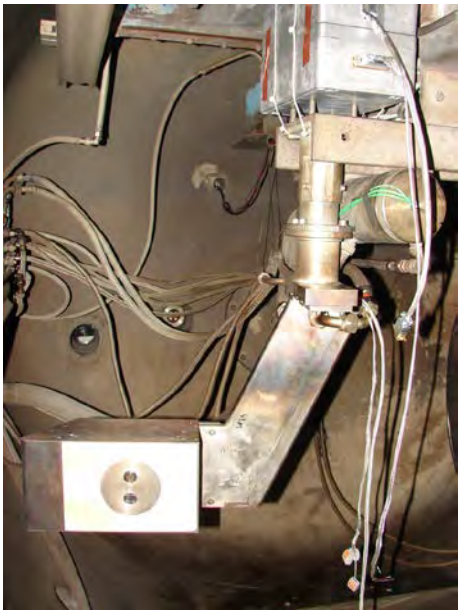

Figure 17: COMARS and radiometer sensors integrated in a flat plate model in L2K

The test conditions have been chosen in such a way, that the concentration of the CO_2 molecules, i.e. radiative heating, could be varied significantly. The enthalpy was varied from 5.6 MJ/kg to 9.2 MJ/kg leading to a CO_2 mole fraction change from 0.546 to 0.227 (Table 3).

Test condition	low enthalpy		high enthalpy	
Configuration	Stagn.	Wedge	Stagn.	Wedge
gas mass flow rate $\dot{m}$ [g/s]	41.2		41.2	
reservoir pressure p_0 [hPa]	790		930	
specific enthalpy h_0 [MJ/kg]	5.6		9.2	
total temperature T_0 [K]	2815		3283	
nozzle throat/exit diameter D_t / D_e [mm]	29/100	29/200	29/100	29/200
distance from nozzle exit x_e [mm]	160	250	160	250
distance from nozzle throat x_t [mm]	329	654	329	654
free stream static pressure p_1 [hPa]	2.1	0.5	2.1	0.4
free stream static temperature T_1 [K]	1001	744	898	604
free stream density ρ_1 [kg/m^3]	$9.4 \cdot 10^{-4}$	$2.7 \cdot 10^{-4}$	$8.6 \cdot 10^{-4}$	$2.5 \cdot 10^{-4}$
free stream velocity v_1 [m/s]	2172	2306	2481	2611
mole fraction of CO_2 n_{CO_2} [–]	0.546	0.546	0.227	0.227
mole fraction of CO n_{CO} [–]	0.277	0.277	0.459	0.459
mass fraction of O_2 n_{O_2} [–]	0.122	0.122	0.162	0.162
mass fraction of O n_O [–]	0.027	0.027	0.126	0.126
mass fraction of N_2 n_{N_2} [–]	0.022	0.022	0.016	0.016
mass fraction of NO n_{NO} [–]	0.005	0.005	0.009	0.009

Table 3: Flow parameters of the aerothermal tests in L2K facility

Figure 18 shows the measured total heat flux rate at both flow conditions in one run. At the beginning of the test the model was positioned outside the flow field and after achieving steady state conditions the model was injected into the flow. The heat flux peaks at the time points 172 and 185 seconds are caused by the heat flux sensor passing through the side shock of the free stream during model injection and removal. The constant heat flux rate between this transition points shows the quality of the flow and reliability of the sensor. The model was re-injected into the flow at a time of 216 seconds after adjusting the flow parameters for the second test condition. Since the total heat flux is proportional to the enthalpy and square root of the stagnation pressure it decreases at low enthalpy flow conditions.

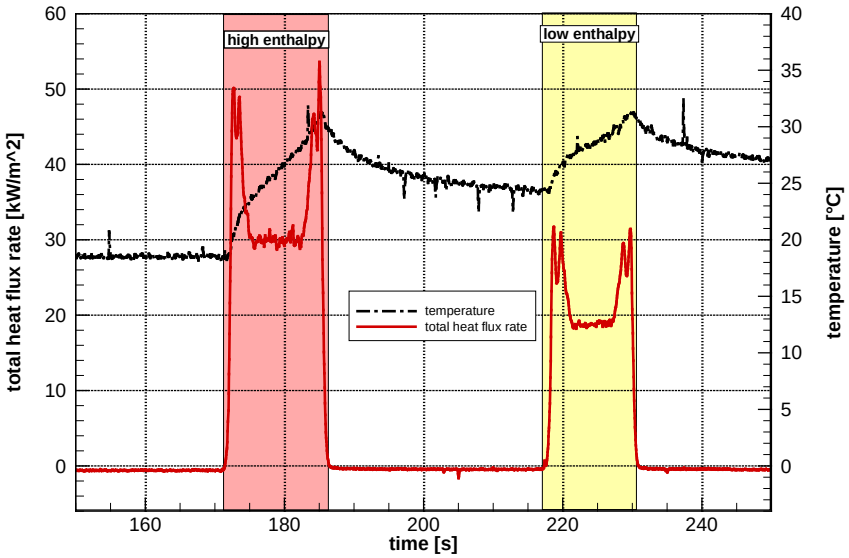

Figure 18: Measured total heat fluxes with the COMARS sensor at two different flow conditions

The situation is different for the radiative heat flux in Figure 19 measured by the DLR broadband radiometer sensor. The radiometer measured the radiative heat flux even without being inside the high enthalpy flow. Therefore the data up to 83 seconds represents the radiation of the free stream at low enthalpy condition. Then the facility parameters electrical current and mass flow rate were varied to reach the high enthalpy flow condition which was achieved at 150 s. Compared to the low enthalpy case the radiative heat flux is lower. This is related to the lower CO_2 concentration. The model was injected into the flow at 175 s. Due to the model leading edge shock the flow density increases and leads to higher radiation compared to the free stream case. After the model was removed from the flow the low enthalpy flow parameters were set again. The injection of the model into the flow at 221 s causes a slight increase in the measured radiative heat flux. But in contrast to the total heat flux, which is mainly convective, the radiative heat flux decreases by increasing the enthalpy due to the decreasing CO_2 concentration.

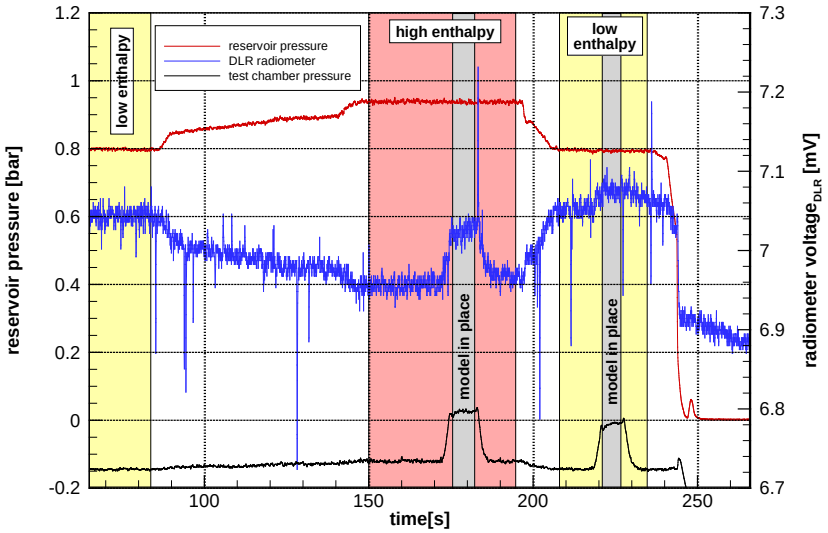

Figure 19: Measured radiative heat fluxes with the radiometer at two different flow conditions

6. CONCLUDING REMARKS

All components of the COMARS+ payload for the ExoMars mission in 2016 were designed and characterized by means of numerical simulations. Aerothermal tests performed at two different flow conditions with Martian atmosphere demonstrated the sensitivity of the COMARS+ sensors to low level total and radiative heat fluxes. The data of complementary spectroscopic measurements in the infrared range showed, that CO_2 molecules are the main contributors of radiation in Martian atmosphere. The qualification tests for the COMARS+ payload components including vibration, shock, thermal / vacuum cycling, EMC and planetary protection requirements are in preparation and will be completed around August 2013.

7. ACKNOWLEDGEMENTS

The authors express their special acknowledgement to the European Space Agency (ESA) and Thales Alenia Space Italy for their support.

8. REFERENCES

[1] A. Gülhan, et al, *The Sharp Edge Flight Experiment SHEFEX I, A Mission Overview*, 5th European Workshop on Thermal Protection Systems and Hot Structures, Noordwijk, Netherlands, 17.-19.5.2006, ESA SP-631.

[2] A. Gülhan, F. Siebe, T. Thiele, D. Neeb, J. Turner, J. Ettl, *Challenges of the SHEFEX-II Flight Instrumentation and Selected Flight Data*, Journal of Spacecraft and Rockets, (accepted, to be published).

[3] A. Gülhan, B. Esser, U. Koch, *Experimental Investigation on Local Aerothermodynamic Problems of Re-entry Vehicles in the Arc Heated Facilities LBK*, AIAA Journal of Spacecraft & Rockets, Volume 38, Number 2, pp. 199-206, March-April 2001.

[4] A. Gülhan, B. Esser, *Arc-Heated Facilities as a Tool to Study Aerothermodynamic Problems of Re-entry Vehicles*, in: Lu, F.K., Marren, D.E. (Eds.): Advanced Hypersonic Test Facilities, Progress in Astronautics and Aeronautics, Vol. 198, pp. 375-403, AIAA, 2002.